Supporting information

In situ chemical transformation synthesis of $Bi_4Ti_3O_{12}$/I-BiOCl 2D/2D heterojunction systems for water pollution treatment and hydrogen production

Kun Qian[a], Li Xia[a], Zhifeng Jiang[b,c,*], Wei Wei[b], Linlin Chen[a], Jimin Xie[a,*]

[a]*School of Chemistry & Chemical Engineering, Jiangsu University, Zhenjiang, 212013, PR China*

[b]*Institute for Energy Research, Center of Analysis and Test, Jiangsu University, Zhenjiang, 212013, PR China*

[c]*school of Life Sciences, The Chinese University of Hong Kong, Shatin, NT, Hong Kong*

Corresponding authors: Zhifeng Jiang & Jimin Xie; Tel.: +86-511-88791708;

Fax: +86-511-88791800;

E-mail: ntjiangzf@sina.com, xiejm391@sohu.com.

Characterization of samples

The crystal structure and phase purity of the prepared samples were analyzed by X-ray diffraction (XRD, Bruker AXS company, Germany). Transmission electron microscopy (TEM, JEM-2010, JEOL), high-resolution TEM (HRTEM) were measured at an accelerating voltage of 300 kV. Scanning electron microscopy (SEM) was performed with a HITACHI S-4800 instrument with an energy-dispersive X-ray spectroscopy (EDS). Ultraviolet-visible (UV-vis) spectroscopy measurements were performed on a UV-2450 ultraviolet-visible spectrophotometer. X-ray photoelectron spectroscopy (XPS) analysis was measured on an ESCALAB MK X-ray photoelectron spectrometer. The fluorescence spectra of the samples were obtained by a QuantaMaster™40 spectrofluorimeter equipped with QuantaMaster & TimeMaster (Photon Technology International, USA). The excitation light employed in recording the fluorescence spectra was 320 nm. The electron spin resonance (ESR) signals of spin-trapped radicals were conducted on a Bruker model ESR JESFA200 spectrometer using spin-trap reagent DMPO in water and methanol, respectively. The photocurrent measurements and electrochemical impedance spectroscopy (EIS) was measured with an electrochemical analyzer (CHI 760B Chenhua Instrument Company).

Photoelectrochemical measurements

The electrochemical measurements were taken by using a conventional three electrode setup connected to an electrochemical station. The preparation method of working electrodes were as follows: 3 mg of the as prepared photocatalysts were suspended in 1 mL of ethylene glycol, followed by sampling 30 μL of the obtained colloidal suspension to drop on a piece of FTO slice. The electrolyte was 0.5 M Na_2SO_4 aqueous solution. And a 300 W Xe lamp was used as the light source of the photoelectrochemical measurements. Electrochemical impedance spectroscopy (EIS) measurements were determined at an AC voltage magnitude of 5 mV with the frequency range of 105-10-1 Hz. A 500W Xe arc lamp was utilized as the light source during the measurements.

Photocatalytic hydrogen production

The photocatalytic hydrogen evolution reaction was carried out in a 100 mL three necked Pyrex flask at ambient temperature and atmospheric pressure, and the outlets of the flask were sealed with silicone rubber septa. A 350 W xenon arc lamp with a UV-cutoff filter (420 nm) was used as light sources to trigger the photocatalytic reaction. The as-prepared sample (50 mg) was dispersed in 80 mL aqueous solution containing 25 vol% methanol for hydrogen evolution. Prior to irradiation, the suspension of the catalyst was dispersed by using an ultrasonic bath for 10 min, and then bubbled with nitrogen through the reactor for 1 h to

completely remove the dissolved oxygen and ensure the reactor was in an anaerobic condition. The reaction temperature was kept at about 293 K. During the whole reaction process, vigorous agitation was performed to ensure the uniform irradiation of the photocatalyst suspension. A 0.4 mL gas was intermittently sampled through the septum, and hydrogen was analyzed by gas chromatography (GC-14C, Shimadzu, Japan, TCD, with nitrogen as a carrier gas and 5 Å molecular sieve column).

Photocatalytic activity for degradation of rhodamine B (RhB), methylene blue (MB), ciprofloxacin (CIP) and tetracycline hydrochloride (TC).

The photocatalytic activities were evaluated by catalyzing the photodegradation of rhodamine B (RhB), methylene blue (MB), ciprofloxacin (CIP) and tetracycline hydrochloride (TC) under visible light irradiation, respectively. The pH value was not adjusted and the experiments were carried out at 25 ^{o}C with a circulating water system to prevent thermal catalytic effects. The photodegradation experiments were performed by adding 50 mg of catalyst into the RhB/MB/CIP/TC solution (10 ppm, 80 mL), respectively. To establish adsorption-desorption equilibrium of the pollutants with the catalyst, the turbid liquid was magnetically stirred for 1 h in the dark. A 350 W xenon arc lamp with a UV-cutoff filter (420 nm) was used as a visible light source. At regular intervals of time, 5 mL of the solution was taken out and centrifuged for

subsequent measurements. The concentration of the clean transparent solution was determined by measuring the absorbance of RhB, MB CIP and TC, whose characteristic absorption peaks were 554 nm (λ_{RhB}), 664 nm (λ_{MB}) , 276 nm (λ_{CIP}) and 365 nm(λ_{TC}), respectively.

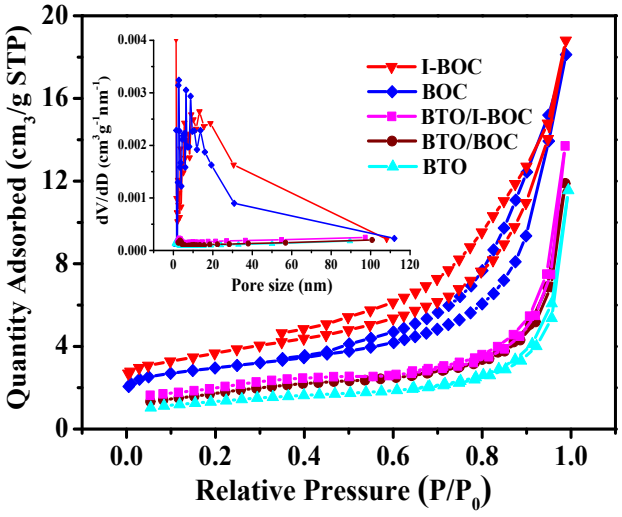

Fig. S1. Nitrogen absorption-desorption isotherms and pore size distribution plot (inset) of the as-prepared samples.

Fig. S1 shows the specific surface area and pore size distribution of the as-prepared samples. All the samples exhibit the type IV isotherms according to the IUPAC classification, demonstrating existence of micropores and mesopores structure. Obviously, BOC and I-BOC microspheres assembled by nanosheets show the largest the BET specific surface area (20.87 cm^2 g^{-1} and 21.55 cm^2 g^{-1}). When introduce the BOC or I-BOC on the surface of BTO, the surface area of the composites shows a slight increase compared with the pure BTO. The specific surface areas and pore sizes data of the as-prepared catalysts calculated by BET and BJH methods were summarized in Table S2. Considering the BET results, it can be concluded that the surface area is not the critical factor to determine the efficiency of the photocatalysts [1,2].

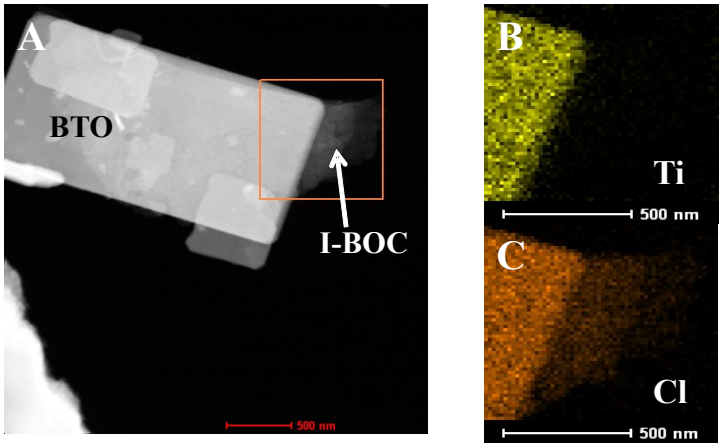

Fig. S2. HAADF-STEM image and the corresponding EDS elemental mapping images of the BTO/I-BOC 2D/2D heterojunction.

Fig. S2 shows the HAADF-STEM image and the corresponding EDS elemental mapping images of the BTO/I-BOC 2D/2D heterojunction. It can be observed that the elemental mapping of Cl shows the same shape with I-BOC and the elemental mapping of Ti appears just in the scope of BTO. BTO and I-BOC can be distinguished easily. Thus, as we thought in TEM and SEM, the rectangular structure with more thickness may be BTO nanosheets, and the circular shape with less thickness may be BOC(I-BOC) nanosheets.

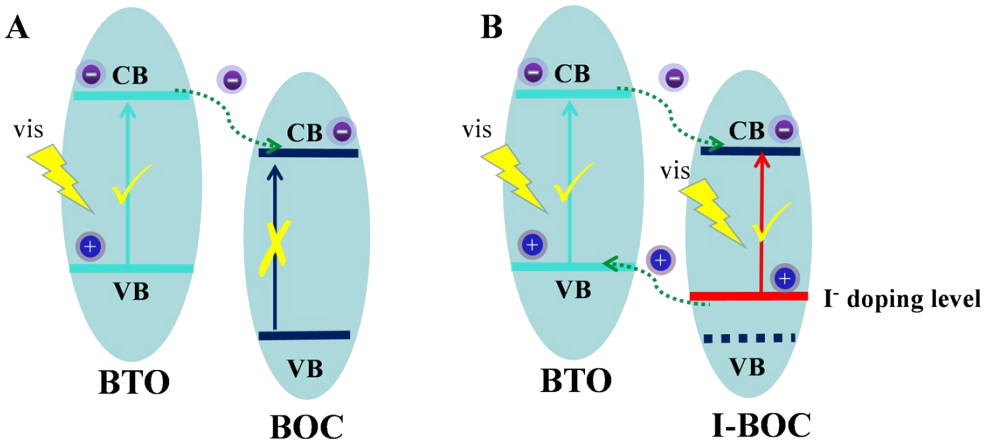

Fig. S3. Photodegradation curves of (A) CIP and (B) TC.

Based on the "Band structure analysis" part, the band structure of BTO/BOC and BTO/I-BOC can be observed in Fig. S3. When BTO/BOC are irradiated with visible light, BTO will generate electron-hole pairs because of the response to visible light. However, BOC can not absorb the visible light. So, the band structure of BTO/BOC may be proposed as Fig. S3A. Because the CB edge potential of BTO is more negative than that of BOC, the excited electron in the CB of BTO tends to transfer to the CB of BOC nanosheet. Then, photogenerated holes are left in the VB of BTO. Thus, charge separation has been achieved. Nevertheless, BTO sample can only be excited by a narrow region of the visible light, the photogenerated and separated electron-hole pairs may be limited. Compared with BTO/BOC, the band structure of BTO/I-BOC may be proposed as Fig. S3B, because both BTO and I-BOC can be excited by visible light. Because the CB edge potential of BTO is more negative than that of I-BOC, the excited electron in the CB of BTO tends to

transfer to the CB of I-BOC nanosheet. At the same time, a great deal of h^+ on the I doped level of I-BOC shifted to that of BTO. Thus, high-efficiency charge separation has been achieved. Compared with BTO/BOC, BTO/I-BOC can generate more electron-hole pairs under visible light irradiation. Then, these photogenerated electron-hole pairs can also be separated efficiently. Thus, the BTO/I-BOC shows more photo-generated carrier separation and transmission efficiency than BTO/BOC.

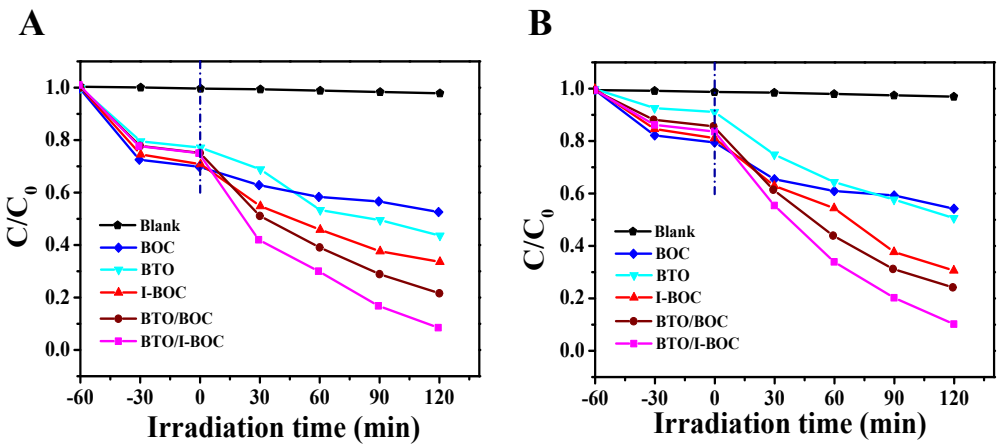

Fig. S4. Photodegradation curves of (A) CIP and (B) TC.

Table S1 The photocatalytic hydrogen production efficiency of different similar photocatalysts.

Photocatalyst	**Light source**	**Reaction conditions**	**HER (μmol/h/g)**	**Ref.**
$NaNb_{0.5}Ta_{0.5}O_3$	150 W Hg UV lamp	0.125 wt% of Pt co-catalyst; Methanol (10%)	37.8	3
g-C_3N_4/$Ca_2Nb_2TaO_{10}$	300 W Xe arc lamp, λ > 420nm	1 wt% of Pt co-catalyst; triethanolamine (10%)	43.5	4
Atomic layer deposition amorphous TiO_2	Asahi Spectra, HAL-C100; λ > 420 nm	1 wt% of Pt co-catalyst; Formic acid (50 %)	52	5
Au nanorod/TiO_2	300 W Xe arc lamp, λ > 420nm	Methanol (20 %)	11.6	6
Black ultrathin BiOCl nanosheets	300 W xenon lamp , λ > 420nm	Triethanolamine (10%)	3.96	7
BiOCl@Au/MnO_x	500-W Xe lamp	Methanol (25 %)	9.6	8

Table S2 The specific surface areas and pore sizes data of the as-prepared photocatalysts.

Samples	**Surface area (m^2/g)**	**Pore size (nm)**
BTO	9.67	3.665
BOC	20.87	1.937
I-BOC	21.55	1.621
BTO/BOC	14.25	4.650
BTO/I-BOC	15.72	3.948

References

[1] Z.Y. Zhang, D.L. Jiang, D. Li, M.Q. He, M. Chen, Appl. Catal. B: Environ. 2016, **183**, 113-123.

[2] T.Y. Wang, W. Quan, D.L. Jiang, L.L. Chen, D. Li, S.C. Meng, M. Chen, Chem. Eng. J. 2016, **300**, 280-290

[3] P. Jana, V. O'Shea, C. M. Montero, P. Gálvez, P. Pizarro, Green Chem., 2015, **17**, 1735-1743.

[4] S. Thaweesak, M. Lyu, P. Peerakiatkhajohn, T. Butburee, B. Luo, Appl. Catal. B, 2017, **202**, 184-190.

[5] P. Zhang, T. Tachikawa, M. Fujitsuka, T. Majima, J. Phys. Chem. Lett., 2016, **7**, 1173-1179.

[6] B. Wu, D. Liu, S. Mubeen, T. T. Chuong, M. Moskovits, G. D. Stucky, J. Am. Chem. Soc., 2016, **138**, 1114-1117

[7] L. Ye, X. Jin, Y. Leng, Y. Su, H. Xie, J. Power. Sources, 2015, **293**, 409-415.

[8] L. Zhang, W. Z. Wang, S. M. Sun, D. Jiang, E. Gao, Appl. Catal. B, 2015, **162**, 470-474.